Research Square

Preprints are preliminary reports that have not undergone peer review.
They should not be considered conclusive, used to inform clinical practice,
or referenced by the media as validated information.

Numerical Optimization of Neon Soft X-ray Emission in a Spherical Plasma Focus Device with Lee Code

M I Nayeem

nayeem4.phy@gmail.com

International University of Business Agriculture and Technology (IUBAT)

M A Malek

Khulna University

Research Article

Keywords: SPF, Current trace fitting, Ne SXR, Electrode geometry, Lee code

Posted Date: January 20th, 2026

DOI: https://doi.org/10.21203/rs.3.rs-8592689/v1

License: This work is licensed under a Creative Commons Attribution 4.0 International License.
Read Full License

Additional Declarations: No competing interests reported.

Version of Record: A version of this preprint was published at Journal of Fusion Energy on August 6th, 2026. See the published version at https://doi.org/10.1007/s10894-026-00596-6.

Numerical Optimization of Neon Soft X-ray Emission in a Spherical Plasma Focus Device with Lee Code

M I Nayeem[1,2*], M A Malek[2]

[1]*Department of Physics, International University of Business Agriculture and Technology (IUBAT), Dhaka-1230, Bangladesh*

[2]*Physics Discipline, Khulna University, Khulna-9208*

*Corresponding author: nayeem4.phy@gmail.com

Abstract: A comprehensive numerical investigation was performed to optimize neon (Ne) soft X-ray emission (Y_{sxr}) from a spherical plasma focus (SPF) device using the latest Lee code. As a prerequisite for predictive modeling, the code was benchmarked against the experimentally measured discharge current waveform of the 135 kJ SPF [1]. In this numerical study using the Lee code (RADPF5.16FIB), the computed current trace is first fitted to the measured one at 14.3 Torr deuterium (D_2) gas and the obtained best-fitted values of the model parameters are found as $f_m = 0.022, f_c = 0.55,\ f_{mr} = 0.14, f_{cr} = 0.14$. These values were then adopted in a systematic optimisation study of the pinch-plasma conditions. The simulations covered Ne fill pressures from 0.5 to 7 Torr, anode and cathode radii at fixed ratios of $b/a = 1.8125$ and $b/a = 1.41$, and charging voltages from 15 to 30 kV. In all the cases, the plasma pinch temperature was constrained to the characteristic neon emission window of $2.3 \times 10^6 – 5 \times 10^6$ K (≈ 200–500 eV). For each electrode geometry the Lee code identified a unique combination of fill pressure and charging voltage that maximized Y_{sxr}. At moderate electrode sizes and bank voltages of 25 kV the SPF is predicted to deliver peak Ne soft X-ray (SXR) yields exceeding 5 kJ per shot with efficiencies greater than 4%. These findings demonstrate that the Lee model code, when calibrated to measured current traces, provides a robust and quantitative tool for the design and scaling of compact, high-performance Ne SXR sources.

Keywords: SPF; Current trace fitting; Ne SXR; Electrode geometry; Lee code.

1. Introduction

The Dense Plasma Focus (DPF) machines are intense pulsed plasma devices, that received much attention since their first operation in the 1960s because of their ability to generate energetic radiation and charged particle beams [2]. The interplay between the current density and its associated magnetic field leads to the collapse of the short-lived plasma, known as the plasma pinching phenomenon in a PF device, belonging to the Z class pinches that generate super-dense (~10^{16}-10^{19} cm^{-3}), super-hot (~1 keV) plasma for a very short time (~100s ns) owing to self-generated electromagnetic compression known as pinch [3], [4]. During this pinch, high-energy ion beam (~MeV) [5], [6] and electron beam (~1 MeV), SXRs (~100s eV) and hard X-rays (100s keV)[7], pulsed fusion neutron (~14.5 MeV) [8] emit. Among the different emissions, SXRs (SXR) play an important role due to their applications in X-ray lithography (using 0.9–1.5 keV photons) [9], [10], [11], [12], contact microscopy (using 0.25–2.5 keV radiation) [13], [14], X-ray radiography [15], [16], and micromachining (using 4 keV photos) [17]. However, efficient production of Ne SXRs requires the plasma to be H-like and He-like in its ionization state and the required pinch temperature lies within the range of approximately 2.3×10^6 to 5×10^6 K (~200–500 eV) [18]. Its identification and characterization and the maintenance of a plasma temperature within this window are the keys to the optimum radiation of the Ne line. The output of a PF device depends sensitively on the operating parameters—filling gas, discharge energy, electrode geometry and charging voltage—which together control the pinch current, radius, density, temperature and confinement time. While numerous experimental studies have been conducted, purely empirical optimization of these variables is time-consuming and costly. Numerical modeling has therefore become indispensable. The Lee model code [19] , in particular, has evolved into a widely used predictive tool because it integrates the dynamic, electrodynamic, thermodynamic and radiation processes of a plasma focus into a single time-dependent framework. When fitted to measured current traces, the code can reproduce the actual behaviour of a given device with high fidelity and then be used to explore parameter variations beyond those yet tested experimentally.

In the present study, the latest Lee model code (RADPF5.16FIB) [20] is applied to the 135 kJ SPF device. The measured discharge current waveform of the SPF was first numerically reproduced to obtain a self-consistent set of dynamic model parameters describing the axial run-down, radial compression and mass-sweeping efficiencies for this device. Using this calibrated model, systematic scans of the Ne filling pressure, electrode geometry and charging

voltage were performed. For each anode–cathode configuration at fixed cathode-to-anode ratios of 1.8125 and 1.41, the code identified the optimum pressure and then the optimum charging voltage that maximize Ne Y_{sxr} while maintaining the pinch plasma within the Ne SXR emission window. The resulting quantitative map of the SPF operating space is presented in this paper as a guide for designing and scaling compact, high-performance Ne SXR sources.

2. Numerical Experiments

A. Soft X-ray Calculation in the Lee Code

The fundamental modeling of the Lee code encompassing with axial and radial phases outlined in 1984 [21], was effectively applied in various numerical studies [22], [23], [24], [25], [26]. The incorporation of radiation-coupled dynamics within a 5-phase code has proven effective for conducting numerical experiments focused on radiation cooling [27]. The five phases are designated as follows: (i) axial phase, (ii) radial inward shock phase, (iii) radial reflected shock (RS) phase, (iv) slow compression (quiescent) or pinch phase, and (v) expanded column phase [28]. The code has seen widespread implementation as an additional feature in several devices, including miniature pinch PF discharges operating at energies as low as 0.1 J, which enables comprehensive simulation capabilities [29]. The specifications, theoretical framework, code implementation, and comprehensive array of outcomes from the "Universal Plasma Focus Laboratory Facility" are readily accessible for download at the specified location [20]. In this work, numerical studies were employed in the latest version of the RADPF5.16FIB code [30]. In the Lee code, the calculation of line radiation Q_L is executed as follows:

$$\frac{dQ_L}{dt} = -4.6 \times 10^{-31} \frac{n_i^2 Z_{eff} Z_n^4 (\pi r_p^2) z_{max}}{T}$$

where, Q_L represents the hydrogen line radiation, Z_n represents the atomic number, Z_{eff} represents the effective number, n_i represents the ion density, r_p represents the pinch radius, z_{max} represents the pinch column length, and T represents the average temperature of the pinch plasma. Here, Y_{sxr} is taken equivalent to the line radiation yield, i.e., $Q_L = Y_{sxr}$.

B. Lee Code Configuration

This paper applies the Lee code which was developed for the Mather-type plasma focus to the spherical plasma focus, which has a geometry different from the Mather-type PF. The Lee model codes designed for a Mather-type configuration with straight coaxial electrodes and a

straight axial acceleration channel of uniform cross-section. The SPF has spherical electrodes with a curved acceleration channel. The electrode geometry has been obtained by applying the 'equivalent straightened electrode' technique to this SPF device [31], [32], [33]. This equivalence could be considered in terms of producing the same run-down time in the code as that observed in the measured current waveform. The measured discharge current trace and the following device parameters of the SPF device are picked out from the published paper [1]:

Bank parameters: Static inductance, L_0 = 36 nH, capacitor bank capacitance, C_o = 432 μF, circuit stray resistance, r_o = 2.3 mΩ.

The tube parameters: Radius of the cathode, b = 14.5 cm, radius of the anode, a = 8 cm,and length of the anode, z_o = 21.3 cm (fitted).

The operating parameters: Operating voltage, V_o = 25 kV, operating pressure, P_o = 1.9×10^3 Pa (~14.3 Torr), operating gas: Neon (Ne).

Fitted model parameters: Axial mass factor (f_m) = 0.022, axial current factor (f_c) = 0.55, radial mass factor (f_{mr}) = 0.14, radial current factor (f_{cr}) = 0.72. The model parameters for the SPF were obtained by fitting the computed and measured current waveforms at a deuterium (D_2) gas pressure of 14.3 Torr (Fig. 1).

To start the numerical studies, the Lee code was configured with the parameters mentioned above. Moreover, the implementation of Ne gas pressure has been investigated as an alternative to D_2, with a comprehensive analysis of its effects on Y_{sxr}.

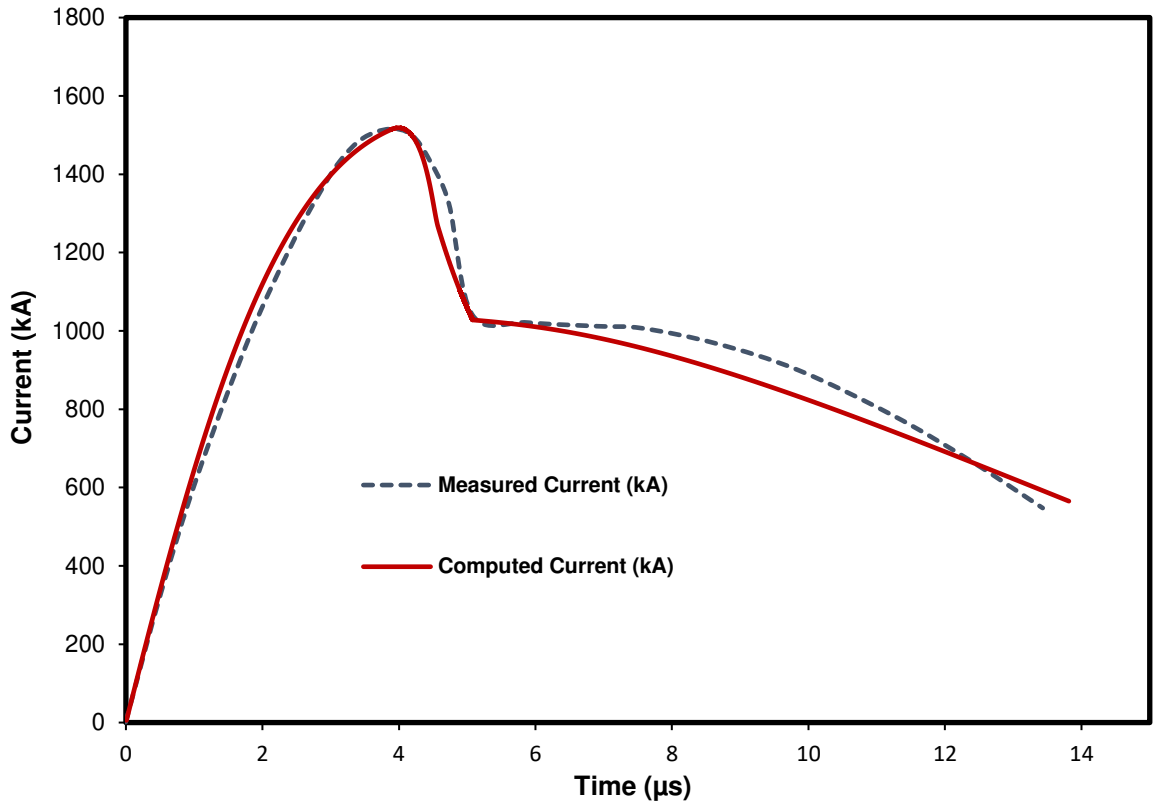


Fig. 1. Current-trace 'fitting' result for SPF to obtain fitted parameters f_m = 0.022, f_c = 0.55, f_{mr} = 0.14, f_{cr} = 0.72 at 14.3 Torr D_2.

3. Results and Discussions

A. SXR yield with pressure variation

The dependence of Y_{sxr} on the Ne filling pressure P_0 for the SPF is presented in Table 1 and Fig. 2, which are configurations simulated with the Lee code. The results indicate a strongly nonlinear variation in Y_{sxr} with P_0, characteristic of the interplay between dynamic plasma compression and radiative losses. At the lowest pressure of 0.5 Torr, the device produces only 46 J per shot, reflecting a relatively low pinch density $\left(n_{i,min} = 0.4 \times 10^{23}\ m^{-3}\right)$ and a relatively large pinch radius (r_p = 1.11 cm) that limits the radiative power. With increasing pressure to 1.0 and 1.5 Torr the pinch current at the collapse increases from 530 - 647 kA, and the radius contracts to 0.87 cm, resulting in improved compression, a longer pinch duration and a rapid rise in Y_{sxr} to 313 J and 1087 J, respectively.

Table 1. Computed outcomes with pressure variation of Ne in the SPF device.

P_0 (Torr)	I_{peak} (kA)	I_{pinch} (kA)	r_p (cm)	z_{max} (cm)	Pinch Duration (ns)	n_i pinch max $10^{23}/m^3$	T_{pinch} ($\times 10^6$) k	Y_{sxr} (J/shot)
0.50	1036	530	1.11	11.9	84.9	0.4	6.42	46.3
1.00	1198	604	1.04	11.9	97.7	1.0	4.34	312.9
1.50	1298	647	0.87	11.9	102.2	2.1	3.37	1087.2
2.00	1371	672	0.52	12.5	116.9	7.8	2.74	3561.3
2.50	**1427**	**691**	**0.48**	**13.1**	**136.9**	**11.5**	**2.31**	**4051.3**
3.00	1473	706	0.54	12.8	139.3	10.7	2.02	3357.6

A further increase in P_0 to 2.0 Torr and 2.5 Torr drives the system into a better parameter space, where the pinch current exceeds 670 kA, the radius shrinks below 0.5 cm and the line density peaks $\left(n_{i,max} = 11.5 \times 10^{23}\ m^{-3}\right)$, producing Y_{sxr} values of 3561 J and a maximum of 4051 J per shot at 2.5 Torr. Beyond this optimum, at 3.0 Torr, the increased mass loading and resistive effects lead to a slight reduction in the effective compression despite a still-rising peak current (706 kA); the pinch duration increases to 139 ns and the temperature decrease to 2.0×10^6 K, resulting in a modest drop in Y_{sxr} to 3358 J. The simulated pinch temperatures across the investigated pressure range (from 6.42×10^6 K at 0.5 Torr decreasing to about 2.31×10^6 K at 2.5 Torr) remain within the characteristic SXR–emitting window for Ne of approximately $2.3 \times 10^6\text{K} - 5 \times 10^6\text{K}$ (200–500eV) [18]. The pronounced maximum in Y_{sxr} at $P_0 = 2.5$ Torr coincides with the regime where the plasma simultaneously achieves its highest line density, strong radial compression (minimum pinch radius), and sufficiently long confinement time to

support efficient collisional–radiative excitation of Ne ions.

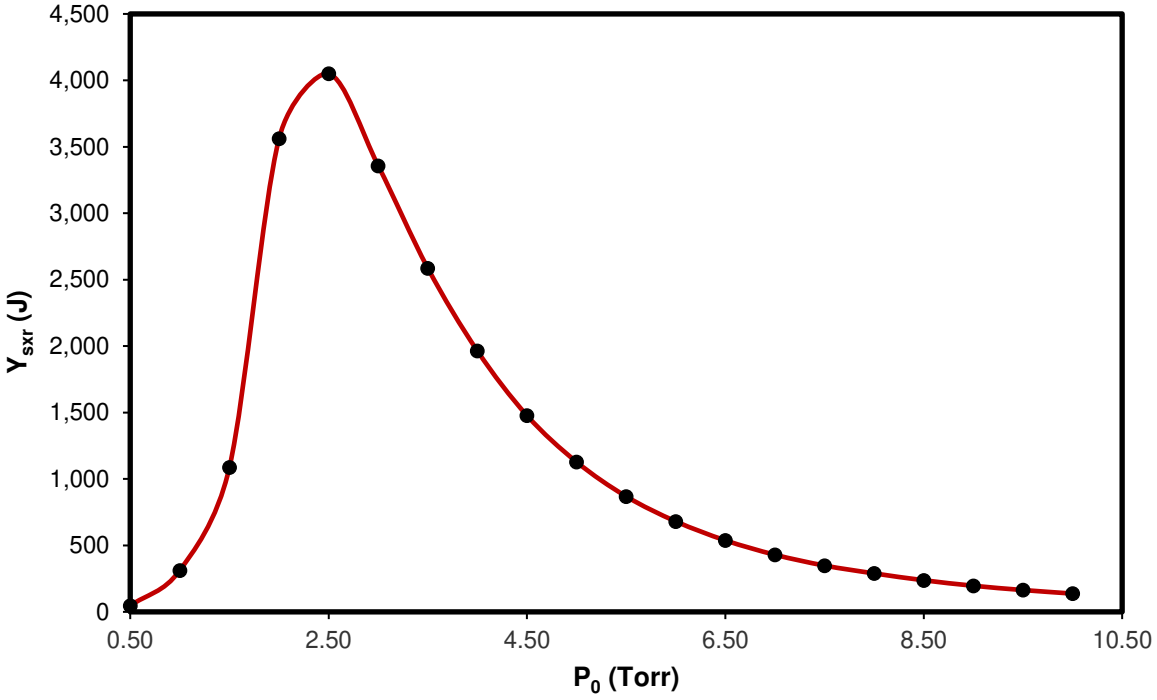


Fig. 2. Computed Y_{sxr} with Ne pressure at 'b = 14.5 cm, and a = 8 cm' in the SPF device.

At higher pressures, the additional mass load and increased resistive damping produce longer current-rise times and lower electron temperatures, thereby reducing the radiative efficiency despite a marginally higher peak current. Conversely, at lower pressures the pinch is undermass-loaded and does not reach the densities required for intense line radiation. The computed behaviour thus indicates that, for the present bank energy, an operating pressure close to 2.5 Torr optimizes the coupled conditions of density, temperature and confinement that govern the conversion of stored energy into Y_{sxr}.

B. SXR Yield with the Electrode Configuration

The influence of the electrode geometry on Y_{sxr} was investigated by varying the anode radius 'a' and cathode radius 'b' independently while holding all other parameters constant. In the first observation (Table 2 and Fig. 3) the cathode radius was fixed at b = 14.5 cm, and the anode radius 'a' was incrementally adjusted between 6.0 and 8.0 cm at the optimum filling pressure of 2.50 Torr. As 'a' increases from 6.0 cm to 7.0 cm the pinch current rises from 668 kA to 683 kA, the pinch radius contracts from 0.59 cm to 0.49 cm and the maximum pinch density increases to 8.3×10^{23} m^{-3}, resulting in a marked increase in Y_{sxr} from only 909 J to 2662 J per shot.

Table 2. Optimized Y_{sxr} with change of 'a' with 'b = 14.5 cm' at P_0 = 2.50 Torr in the SPF device.

a (cm)	I_{peak} (kA)	I_{pinch} (kA)	r_p (cm)	z_{max} (cm)	Pinch Duration (ns)	n_i pinch max $10^{23}/m^3$	T_{pinch} (× 10^6) k	Y_{sxr} (J/shot)
6.0	1246	668	0.59	8.9	70.2	4.2	3.80	909.9
7.0	1336	683	0.49	10.5	88.3	8.3	2.95	2662.4
7.8	1409	689	0.45	12.8	130.5	12.2	2.42	4038.9
7.9	**1419**	**690**	**0.46**	**13.0**	**134.4**	**11.9**	**2.37**	**4064.9**
8.0	1427	691	0.48	13.1	136.9	11.5	2.31	4051.3

A further reduction in the pinch radius to 0.46 cm at a = 7.9 cm yields the maximum Y_{sxr} of 4065 J/shot with =134 ns and the temperature has almost not ceased being within the SXR-emitting regime (T_{pinch} = 2.37 × 10^6 K). Beyond this point, at a = 8.0 cm the pinch parameters are again similar to those above but Y_{sxr} drops slightly to 4051 J, suggesting that the configuration around a ≈ 7.9 cm provides the most optimal trade-off between current and compression and confinement for Y_{sxr} under these conditions.

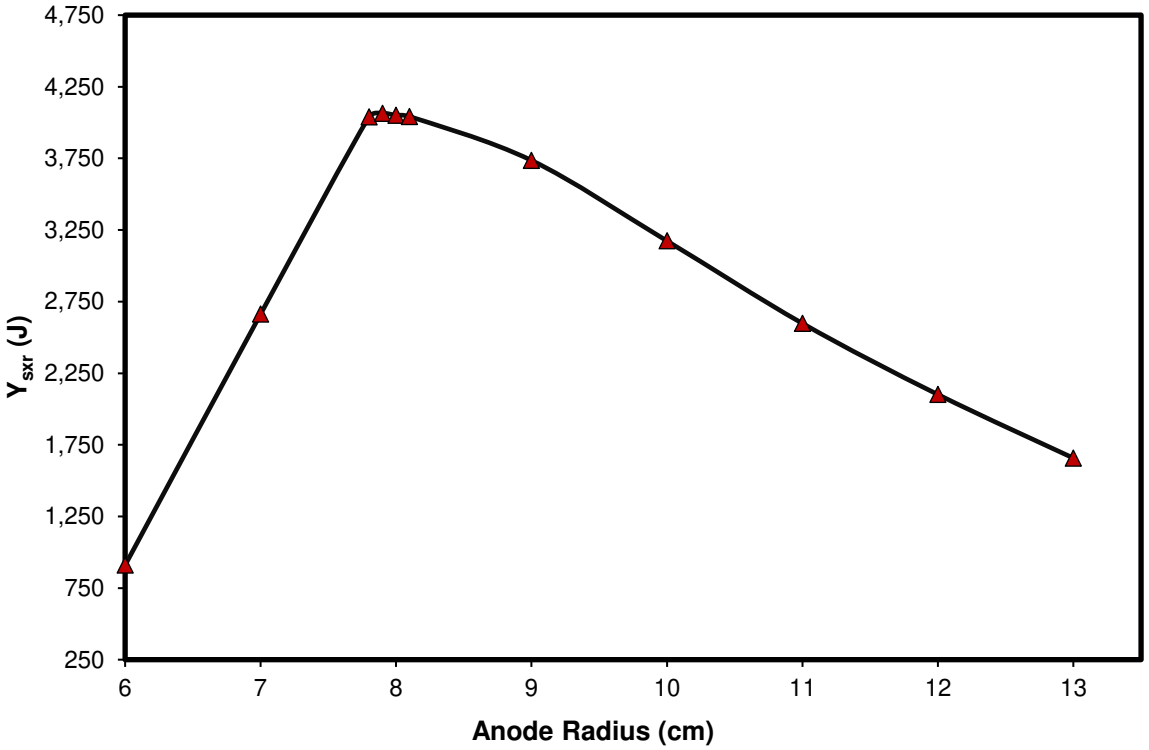


Fig. 3. Optimized Y_{sxr} with Ne pressure with change of 'a' at b = 14.5 cm in the SPF device.

In the second observation (Table 3 and Fig. 4), the anode radius a = 8.0 cm was kept constant and the cathode radius 'b' was changed from 10.1 cm to 14.0 cm, at again P_0 = 2.50 Torr. Table

3 shows that by targeting 'b' to keep it in the range of 10.1–11.1 cm, both high I_{peak} = 720 kA and high r_p = 0.49 cm can be achieved with a pinch duration of 142 ns, providing a Y_{sxr} maximum (4703 J/shot) when 'b' = 11.1 cm.

Table 3. Optimized Y_{sxr} with change of 'b' with 'a = 8 cm' at P_0 = 2.50 Torr in the SPF device.

b (cm)	I_{peak} (kA)	I_{pinch} (kA)	r_p (cm)	z_{max} (cm)	Pinch Duration (ns)	n_i pinch max $10^{23}/m^3$	T_{pinch} ($\times 10^6$) k	Y_{sxr} (J/shot)
10.1	1539	736	0.53	12.8	129.0	9.4	2.63	4567.9
10.2	1536	735	0.53	12.8	129.3	9.5	2.62	4563.1
10.5	1523	730	0.52	12.9	131.5	9.9	2.58	4564.7
11.0	1506	723	0.49	13.2	140.4	11.0	2.53	4682.6
11.1	**1504**	**722**	**0.49**	**13.3**	**141.9**	**11.1**	**2.53**	**4702.5**
11.2	1500	720	0.49	13.2	141.0	11.1	2.52	4659.3
12.0	1478	712	0.48	13.2	139.8	11.3	2.46	4487.4
13.0	1454	702	0.48	13.1	137.4	11.3	2.39	4273.6
14.0	1436	694	0.48	13.1	136.2	11.4	2.34	4106.0

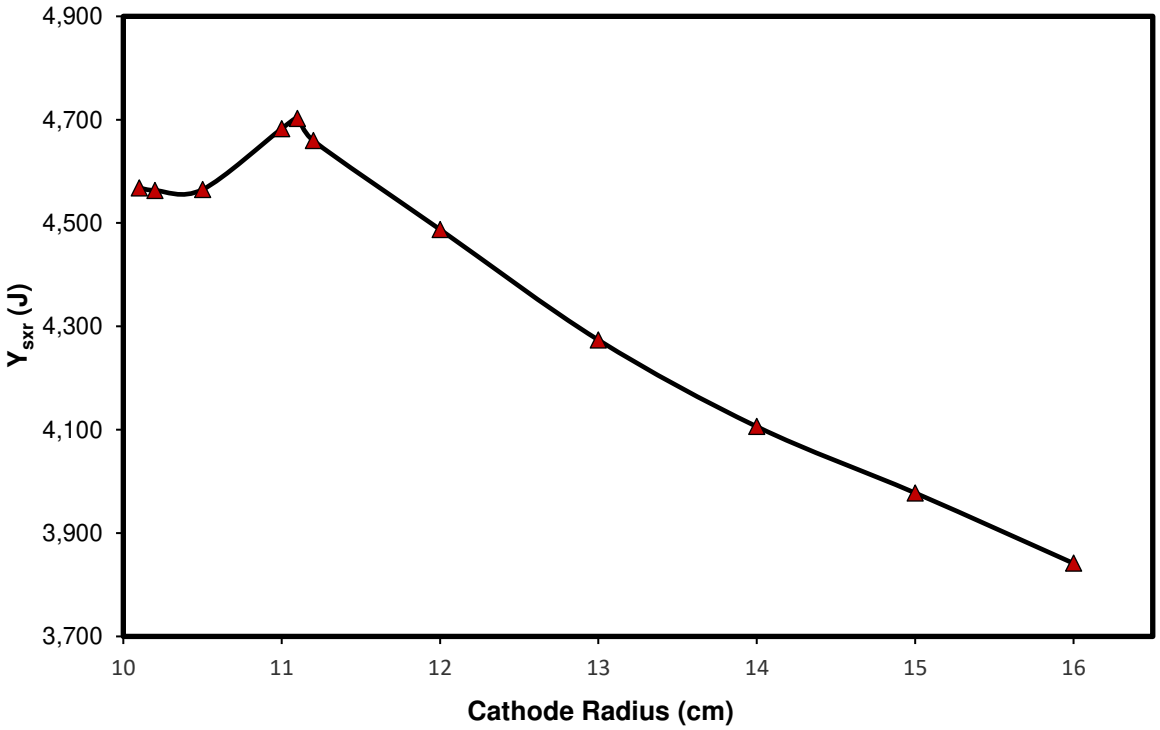


Fig. 4. Optimized Y_{sxr} with Ne pressure with change of 'b' at a = 8 cm in the SPF device.

Both the pinch duration and radius are smaller at greater cathode radii (12 - 14 cm), with a consequent reduction in the pinch temperature from 2.53 × 10^6 K to 2.34 × 10^6 K, leading to a

decrease in Y_{sxr} to 4106 J per shot at b =14.0 cm. These results demonstrate that the electrode configuration strongly influences the PF dynamics and thus the SXR emission. Optimizing the anode–cathode geometry modifies the inductance and current sheath acceleration, which in turn affect the pinch current, radius, density and temperature. Under the present bank and pressure conditions, the configuration of a ≈ 7.9 cm and b ≈11.1 cm provides the best combination of high density, suitable pinch temperature (within 200–500 eV) and adequate confinement time for maximising Y_{sxr}.

After the optimal electrode configuration (a = 7.9 cm, b = 11.1 cm, $b/a = 1.41$) was determined, a systematic variation in the Ne fill pressure P_0 was pursued to determine the maximum achievable Y_{sxr} under such conditions. The summarized results are presented in Table 4 and Fig. 5. At sub-optimal pressures (0.5–1.0 Torr), the device produces only 40–260 J per shot due to inadequate mass loading, relatively large pinch radii of 1.13–1.07 cm and therefore a moderate peak ion density (< 1×10^{23} m^{-3}). Gradual increments in P_0 improve the axial current sheath drive and compression, with the pinch current increasing from 547 kA at 0.5 Torr to 729 kA at 2.75 Torr as the pinch radius contracts to ≈ 0.50 cm and the peak ion density reaches 11.5×10^{23} m^{-3}.

Table 4. Optimized Y_{sxr} with P_0 variation at 'b = 11.1' cm and 'a = 7.9' cm in the SPF device.

P_0 (Torr)	**I_{peak} (kA)**	**I_{pinch} (kA)**	**r_p (cm)**	**z_{max} (cm)**	**Pinch Duration (ns)**	**n_i pinch max $10^{23}/m^3$**	**T_{pinch} (× 10^6) k**	**Y_{sxr} (J/shot)**	**Efficiency %**
0.50	1073	547	1.13	11.8	82.8	0.4	6.93	39.6	0.03
0.75	1171	592	1.10	11.8	89.7	0.6	5.55	117.1	0.09
1.00	1245	625	1.07	11.8	95.6	0.9	4.73	259.8	0.19
1.15	1281	641	1.04	11.8	98.0	1.1	4.35	388.7	0.29
1.25	1302	650	1.02	11.8	99.5	1.2	4.14	497.1	0.37
1.50	1353	671	0.95	11.8	101.8	1.7	3.70	869.9	0.64
1.75	1394	688	0.85	11.8	103.1	2.5	3.35	1445.0	1.07
2.00	1430	701	0.70	11.9	106.1	4.2	3.05	2461.5	1.82
2.25	1463	712	0.53	12.4	119.0	8.1	2.80	3976.6	2.95
2.50	1492	721	0.51	12.5	123.1	9.8	2.59	4265.9	3.16
2.75	**1518**	**729**	**0.50**	**13.0**	**138.2**	**11.5**	**2.40**	**4441.4**	**3.29**
3.00	1542	737	0.52	12.9	140.2	11.3	2.25	4180.4	3.10

This trend is combined with a significant increase in $Y_{sxr,}$ increasing from 870 J at 1.5 Torr to 2462 J at 2.0 Torr and up to 4266 J at 2.5 Torr. The SXR yield reaches its peak value of 4441 J at P_0 = 2.75 Torr, corresponding to the longest confinement time (138 ns) and to the highest overall energy conversion efficiency (3.29% of stored energy). In addition to this pressure, further mass loading and resistive damping decrease to 2.25 × 10^6 K and cause a small drop in Y_{sxr} to 4180 J at 3.0 Torr. The calculated pinch temperatures during the scan lie in the typical Ne SXR–emitting window, which is consistent with a high pinch current, small pinch radius, high plasma density and long confinement time being required for peak emission.

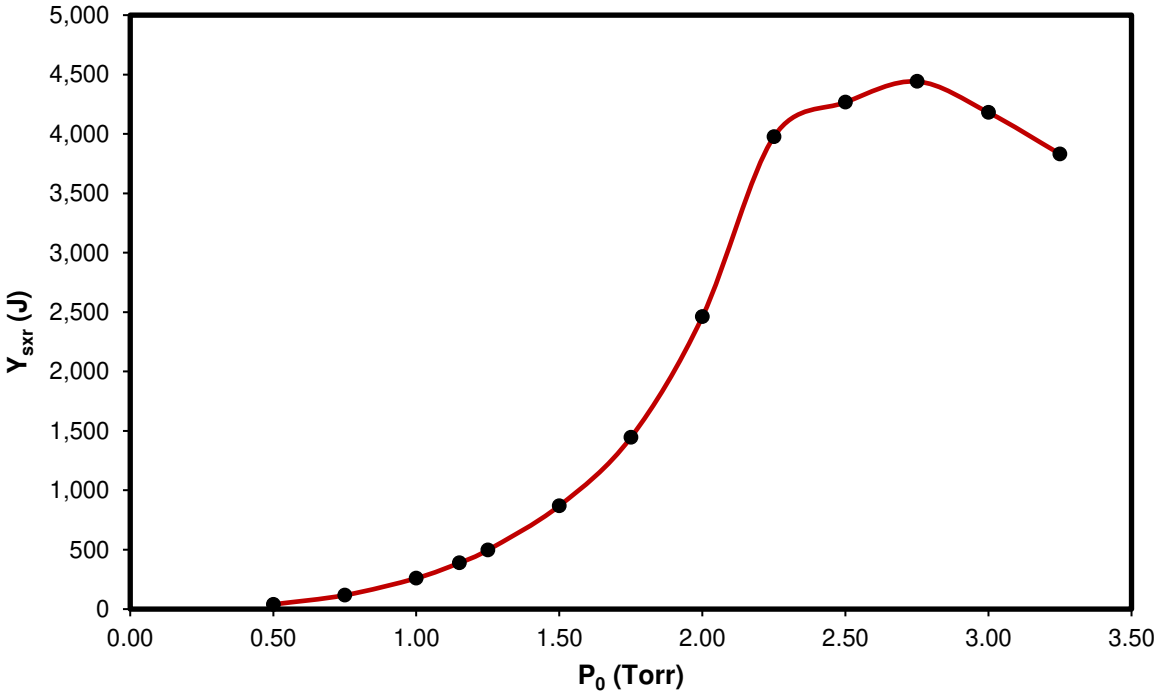


Fig. 5. Optimized Y_{sxr} with Ne pressure at b = 11.1 cm, and a = 7.9 cm in the SPF device.

These findings show that, once the electrode configuration is optimized, by further tuning of the filling pressure it is possible to increase Y_{sxr} by an additional ≈ 10% and obtained P_0 ≈ 2. 75 Torr as the optimal operation point for SXR emission in this SPF device.

C. Optimization of Y_{sxr} by Scaling Electrode Geometry at b/a = 1.8125 and 1.41

To systematically study the impact of electrode scaling on SXR generation, a series of simulations with different anode radii and cathode radii were performed at a constant ratio of the cathode radius to the anode radius b/a = 1.8125. The Lee code was executed as a function of Ne fill pressure (0.5–7.0 Torr) for various electrode geometries in order to obtain knowledge about the pressure dependence of the PF parameters and to pinpoint an optimal working point

for Y_{sxr} at each particular electrode setup. The highest yield values and best pressures that were found in these analyses are illustrated in Fig. 6 and Fig. 7 and are listed in Table 5.

Table 5. Optimized Y_{sxr} at different anode-cathode radii with ratios of 1.8125 and 1.41 with the optimum pressure of Ne in the SPF device.

$b/a = 1.8125$					$b/a = 1.41$				
a (cm)	**b (cm)**	**P_0 (Torr)**	**Y_{sxr} (J)**	**Efficiency %**	**a (cm)**	**b (cm)**	**P_0 (Torr)**	**Y_{sxr} (J)**	**Efficiency %**
12.3	22.294	0.75	4809	3.56	13.1	18.471	0.5	791	0.6
10	18.125	1.25	4834	3.58	**10.8**	**15.228**	**1.15**	**5413**	**4.01**
8.8	15.95	1.75	4503	3.34	9.2	12.972	1.75	5118	3.80
8	14.5	2.25	4226	3.13	8.8	12.408	2	4982	3.69
7.7	13.9562	2.5	4126	3.06	8.4	11.844	2.25	4795	3.55
7	12.6875	3.25	3722	2.76	7.5	10.575	3	4354	3.23
6.7	12.14375	3.75	3390	2.51	6.9	9.729	3.75	3876	2.87
6.3	11.41875	5	4321	2.22	6.6	9.306	4.25	3632	2.69
6	10.875	4.25	2027	2.21	6.3	8.883	4.75	3465	2.57
5.8	10.5125	4.5	2868	2.12	6.1	8.601	4.5	3329	2.47
5.6	10.15	5	2767	2.05	5.9	8.319	5	3232	2.39
5.4	9.7875	5.25	2660	1.97	5.7	8.307	5.25	3074	2.28
5.3	9.60625	5.5	2608	1.93	5.5	7.755	5.25	2937	2.18
5	9.0625	5.75	2475	1.83	5.3	7.473	6	2873	2.13
4.9	8.88125	6	2433	1.74	5.1	7.191	6	2780	2.06

The findings demonstrate that while the device can maintain high SXR emission over a wide range of electrode sizes while maintaining a 1.8125 ratio, the absolute optimum pressure varies with geometry. For the highest configuration (a = 12.3 cm, b = 22.3 cm), for instance, the Lee code forecasts a maximum Y_{sxr} of 4809 J per shot at an optimal pressure of 0.75 Torr with an efficiency of 3.56%. By decreasing the electrode dimensions to a = 10.0 cm and b = 18.125 cm, and adjusting the pressure, a new optimum is identified at P_0 = 1.25 Torr, where the yield reaches a maximum of 4834 J (3.58%). A further decrease to a = 8.8 cm, b = 15.95 cm yields an optimum at 1.75 Torr with 4503 J (3.34%), whereas at a = 8.0 cm, b = 14.5 cm, the optimum shifts to 2.25 Torr with 4226 J (3.13%). Throughout this development, the pinch current increases, the pinch radius decreases, and the plasma density increases, whereas the pinch temperatures are sustained within the distinctive SXR-emitting range of 200–500 eV (2.3–5 $\times 10^6$ K).

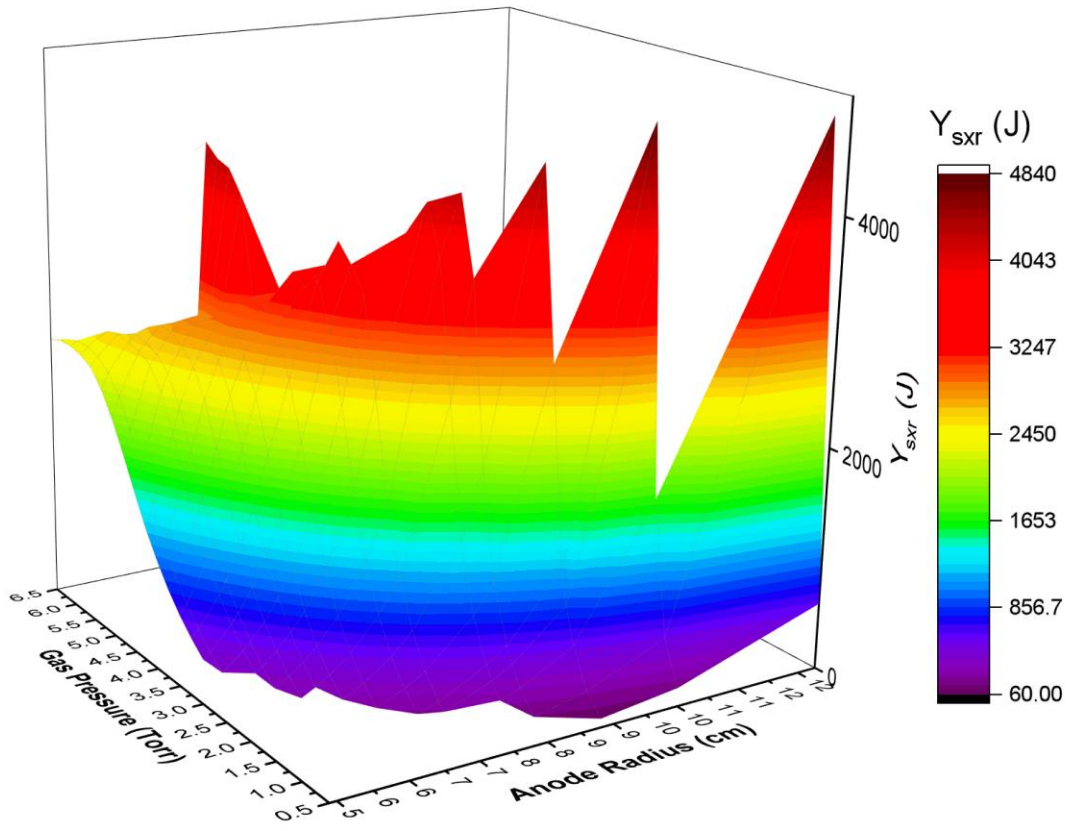


Fig. 6. Computed Y_{sxr} with respect to different anode cathode radii (b/a = 1.8125) and Ne gas pressures in the SPF device.

The yields progressively decrease from ~ 4.1 kJ to ~ 2.6 kJ per shot at even lower anode radii, when the ideal pressures shift into the 2.5–5.0 Torr region. This decline indicates the initiation of mass loading and a subsequent decrease in electron temperature and confinement time, notwithstanding the elevated peak currents. The efficiencies are still approximately 2–3 %, though, which shows that a stable b/a ratio still helps with good current sheath dynamics, even on a tiny scale. These findings indicate that a geometric scaling law is robust when the cathode-to-anode radius ratio is maintained at 1.8125. Specifically, an optimum pressure exists for each absolute electrode size, which, when determined through pressure variation, results in the highest possible Y_{sxr}. Under the examined conditions, the device attains optimal yields (approximately 4.8–4.9 kJ per shot) and efficiencies (exceeding 3.5%) at moderate electrode dimensions (anode radii of 8–12 cm) with pressures ranging from 0.75 to 2.25 Torr. This method provides a viable pathway for the construction and expansion of PF devices to improve Ne SXR output.

In a second series of simulations the electrode radii were scaled while maintaining a fixed cathode-to-anode radius ratio of b/a =1.41. For each configuration the Lee code was run over a Ne fill-pressure range of 0.5–7.0 Torr to map the variation in the plasma parameters and determine the optimum pressure for Y_{sxr}. The peak yields and their corresponding operating conditions are summarized in Table 5 and illustrated in Fig. 7.

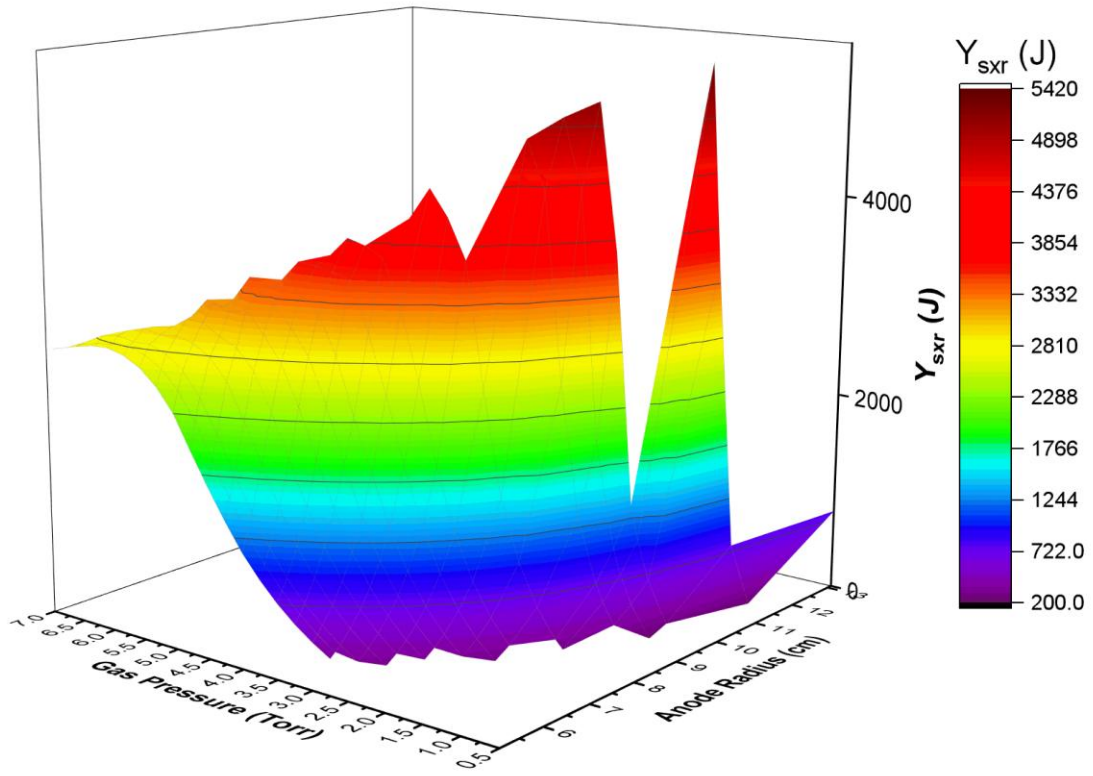


Fig. 7. Computed Y_{sxr} with respect to different anode cathode radii (b/a = 1.41) and Ne gas pressures in the SPF device.

The findings indicate that, similar to the 1.8125 ratio, a consistent ratio of 1.41 results in high Y_{sxr}, albeit with a distinct pattern of ideal pressures. A maximum Y_{sxr} of 5413 J per shot at P_0 = 1.15 Torr with an efficiency of 4.01% is obtained by the pressure variation for the largest electrodes (a = 10.8 cm, b= 15.2 cm). The optimum is shifted to 1.75 Torr with 5118 J (3.80 %) when the electrode size is reduced to a = 9.2 cm, b = 12.97 cm, whereas a = 8.8 cm, b = 12.41 cm gives 4982 J at 2.0 Torr (3.69 %). The yield reaches its maximum at 4795 J at 2.25 Torr (3.55%) at intermediate geometries, such as a = 8.4 cm and b = 11.84 cm. The peak Y_{sxr} values progressively decrease from approximately 4.35 kJ to approximately 3.0 kJ per shot as the anode radius is further reduced (7.5–6.1 cm), and the optimal pressures shift to 2.5–4.25

Torr. Even though the pinch current is still high, this decrease is caused by the start of over-mass loading and increased resistive losses, which lower the electron temperature and shorten the confinement time. However, during these scans, the calculated pinch temperatures remain within the typical 200–500 eV (≈ $2.3 \times 10^6 - 5 \times 10^6$ K) Ne SXR emission range, confirming that the observed maxima are the result of favorable current, density, and temperature combinations.

These findings show that, for moderate electrode sizes and lower pressures, the device can achieve even higher peak yields than at 1.8125 at a cathode-to-anode ratio of 1.41, with Y_{sxr} exceeding 5.4 kJ per shot and efficiencies above 4%. The systematic pressure scans reveal that there is an ideal pressure for every electrode configuration where the combined factors of high pinch current, small pinch radius, high plasma density, and adequate confinement time result in the highest Y_{sxr}. This proves that the Lee code can be used to map the operating space and find the best geometry and pressure combination for better Ne SXR emission.

D. SXR yield Optimization with Cathode to Anode Ratios of 1.8125 and 1.41

After the ideal Ne filling pressure for each anode-cathode shape that maximizes Y_{sxr} was identified (Table 5, Figs. 6–7), the optimization research was expanded to examine at how the charging voltage affects the SPF device. The reason for this step was that the amount of plasma compression, the electron temperature, and eventually the SXR output are all significantly influenced by the stored energy and current rise-time controlled by the charging voltage, even at a given electrode geometry and ideal gas pressure. Therefore, the Lee code was run throughout a charging-voltage range of 15-30 kV for each electrode design at its previously established optimum pressure to identify the voltage at which Y_{sxr} is maximized. The peak yields and efficiencies are are displayed in Figs. 8 and 9, and summarized in Table 6.

For the configuration with a fixed ratio of b/a = 1.8125 (Table 6 and Fig. 8) the SPF device maintains a high Y_{sxr} across a wide range of anode radii and voltages. The highest Y_{sxr} of 4809 J per shot is achieved at V_0 = 25 kV with an efficiency of 3.56% at the largest geometry (a = 12.3 cm, b = 22.3 cm). A yield of 4178 J (3.65%) is achieved by reducing the electrodes to a = 10 cm,and b = 18.125 cm and adjusting the voltage to 23 kV. Intermediate anode radii of 8.8–7.7 cm and V_0 = 24–25 kV allow yields of 4.1–4.2 kJ per discharge. The output gradually decreases to roughly 2.4 kJ below an anode radius of approximately 6.5 cm.

Table 6. Optimized Y_{sxr} at different anode-cathode radius with a ratio of 1.8125 and 1.41 with optimum operating voltage for Ne in the SPF device.

$b/a = 1.8125$					$b/a = 1.41$				
a (cm)	**b (cm)**	**V_0 (kV)**	**Y_{sxr} (J)**	**Efficiency %**	**a (cm)**	**b (cm)**	**V_0 (kV)**	**Y_{sxr} (J)**	**Efficiency %**
12.3	22.294	25	4809	3.56	13.1	18.471	22	1986	1.90
10	18.125	23	4178	3.65	**10.8**	**15.228**	**25**	**5413**	**4.01**
8.8	15.95	24	4163	3.35	9.2	12.972	24	4736	3.81
8	14.5	25	4226	3.13	8.8	12.408	25	4982	3.69
7.7	13.9562	25	4126	3.06	8.4	11.844	25	4795	3.55
7	12.6875	25	3722	2.76	7.5	10.575	25	4354	3.23
6.7	12.14375	26	3667	2.51	6.9	9.729	25	3876	2.87
6.3	11.41875	27	3554	2.26	6.6	9.306	25	3632	2.69
6	10.875	23	2614	2.29	6.3	8.883	25	3465	2.57
5.8	10.5125	23	2539	2.22	6.1	8.601	23	2871	2.51
5.6	10.15	23	2343	2.05	5.9	8.319	25	3232	2.39
5.4	9.7875	25	2660	1.97	5.7	8.307	25	3074	2.28
5.3	9.60625	25	2608	1.93	5.5	7.755	22	2382	2.28
5	9.0625	25	2475	1.83	5.3	7.473	25	2873	2.13
4.9	8.88125	25	2434	1.80	5.1	7.191	25	2780	2.06

This is because the geometry becomes less optimal and greater voltages (up to 27 kV) are needed. As the electrode scale varies, this behavior illustrates how the current rise-time, dynamic inductance, and mass loading interact differently. The computed pinch temperatures remain within the typical Ne SXR emission window of 200–500 eV ($\approx 2.3 \times 10^6 - 5 \times 10^6$ K) across these operating points, suggesting that variations in Y_{sxr} are caused by confinement time, pinch current, radius, and plasma density rather than a break from the radiative regime.

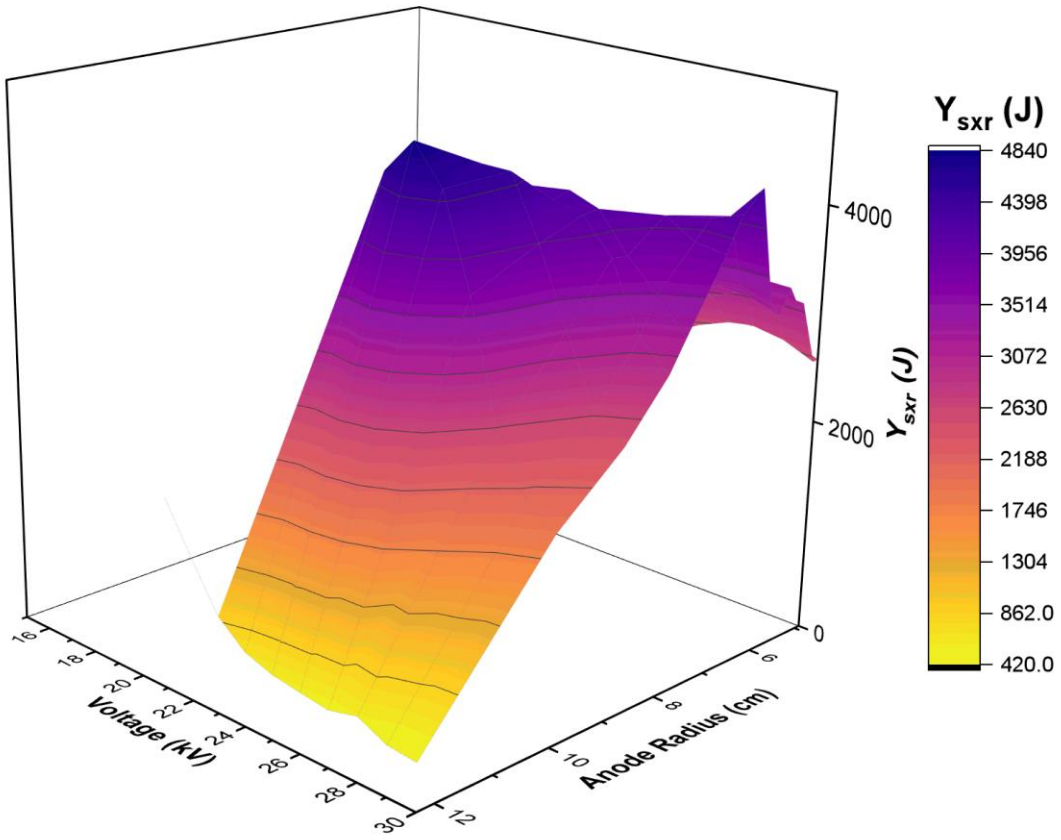


Fig. 8. Computed Y_{sxr} with respect to different anode cathode radii (b/a = 1.8125) and operating voltages with the optimum Ne gas pressure in the SPF device.

The same procedure was implemented for the configuration with a fixed ratio of b/a = 1.41 (Fig. 9 and Table 6). This configuration results in even greater peak yields at moderate electrode diameters. At a = 10.8 cm, b = 15.228 cm, the highest Y_{sxr} of 5413 J per shot is reached at V_0 = 25 kV (4.01%). At a = 9.2 cm, b = 12.97 cm and V_0 = 24 kV, it reaches 4736 J (3.81%). As the pinch current and temperature decrease despite same mass loading, the yield steadily decreases at smaller anodes and lower voltages, but it remains above 4.3–4.9 kJ per shot across the range of 8.8–7.5 cm anode radii at 25 kV. The calculated pinch temperatures in each case fall within the 200–500 eV Ne SXR–emitting window, confirming that the maxima result from the best possible combinations of high pinch current, small pinch radius, elevated density, and adequate confinement time. Moreover, once the ideal pressure for each geometry has been determined, additional charging voltage tuning can greatly increase Y_{sxr}. The most advantageous working conditions for the SPF device under study are a voltage of 25 kV and a

modest electrode size (a = 10.8 cm, b = 15.228 cm), which produce SXR outputs above 5 kJ per shot and efficiencies close to 4%.

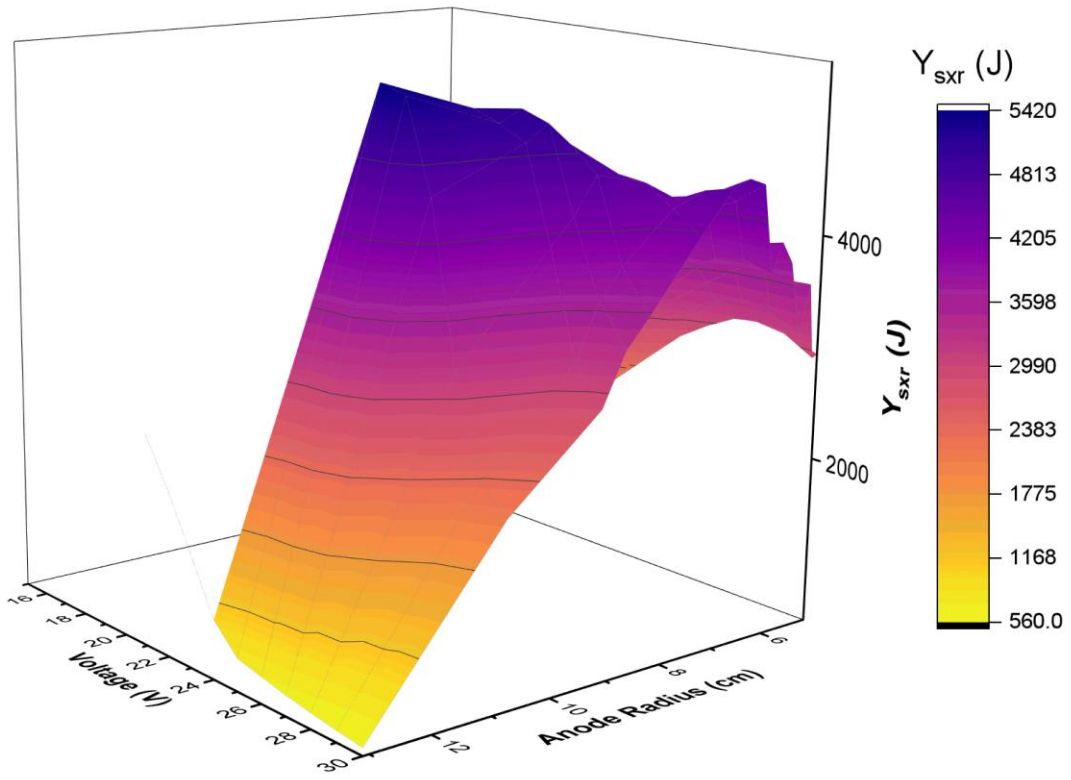


Fig. 9. Computed Y_{sxr} with respect to different anode cathode radii (b/a = 1.41) and operating voltages with the optimum Ne gas pressure in the SPF device.

4. Conclusion

This study presents a self-consistent, code-based optimization of Ne SXR production from an SPF device. The modeling commenced with an accurate reproduction of the measured discharge current waveform of the 135 kJ SPF device, from which the dynamic Lee-code model parameters were determined as $f_m = 0.022, f_c = 0.55,\ f_{mr} = 0.14, f_{cr} = 0.14$. Using this calibrated model, extensive parameter scans were performed across Ne fill pressures, electrode geometries and charging voltages. For each anode–cathode configuration at fixed b/a ratio the optimum Ne pressure was first identified, and then the charging voltage was varied to establish the voltage at which Y_{sxr} is maximized while maintaining the pinch temperature within the 2.3

$\times 10^6 - 5 \times 10^6$ K (200–500 eV) emission window. The analysis shows that at moderate electrode dimensions and bank voltages of 25 kV the SPF can achieve Y_{sxr} exceeding 5 kJ per shot with efficiencies of 3–4%. The results provide clear scaling relationships linking the fill pressure, electrode geometry and charging voltage to achieve Ne Y_{sxr} and demonstrate that a Lee-code model calibrated to measured current traces can reliably guide the optimization and scaling of SPF devices as compact, high-brightness SXR sources.

Acknowledgement

The author acknowledges his heartfelt appreciation to Dr. Sing Lee for granting access to the Lee Code and the Physics Department, IUBAT for providing the sound environment.

References

[1] N. V. Zavyalov *et al.*, "A source with a 1013 DT neutron yield on the basis of a spherical plasma focus chamber," *Plasma Phys. Rep.*, vol. 39, no. 3, pp. 243–247, Mar. 2013, doi: 10.1134/S1063780X12120070.

[2] J. W. Mather, "Dense Plasma Focus Methods of Experimental Physics," in *New York: Academic, 9B*, R. Lovberg and H. Griew, Eds., 187, 1971.

[3] J. W. Mather, "15. Dense Plasma Focus," in *Methods in Experimental Physics*, vol. 9, R. H. Lovberg and H. R. Griem, Eds., in Plasma Physics, vol. 9. , Academic Press, 1971, pp. 187–249. doi: 10.1016/S0076-695X(08)60862-5.

[4] J. W. Mather, "Formation of a High-Density Deuterium Plasma Focus," *The Physics of Fluids*, vol. 8, no. 2, pp. 366–377, Feb. 1965, doi: 10.1063/1.1761231.

[5] E. Boggasch *et al.*, "*z* -pinch plasma lens focusing of a heavy-ion beam," *Phys. Rev. Lett.*, vol. 66, no. 13, pp. 1705–1708, Apr. 1991, doi: 10.1103/PhysRevLett.66.1705.

[6] V. Fortov *et al.*, "The application of high intensive Z-pinch radiation and heavy ion beams for research on high energy density physics," in *12th International Conference on High-Power Particle Beams. BEAMS'98. Proceedings (Cat. No.98EX103)*, Haifa, Israel: IEEE, 1998, pp. 89–94. doi: 10.1109/BEAMS.1998.822395.

[7] N. R. Pereira and J. Davis, "X rays from *z* -pinches on relativistic electron-beam generators," *Journal of Applied Physics*, vol. 64, no. 3, pp. R1–R27, Aug. 1988, doi: 10.1063/1.341808.

[8] A. L. Velikovich *et al.*, "Z-pinch plasma neutron sources," *Physics of Plasmas*, vol. 14, no. 2, p. 022701, Feb. 2007, doi: 10.1063/1.2435322.

[9] Y. Kato, I. Ochiai, Y. Watanabe, and S. Murayama, "Plasma focus x-ray source for lithography," *Journal of Vacuum Science & Technology B: Microelectronics Processing and Phenomena*, vol. 6, no. 1, pp. 195–198, Jan. 1988, doi: 10.1116/1.584044.

[10] S. Lee *et al.*, "High rep rate high performance plasma focus as a powerful radiation source," *IEEE Transactions on Plasma Science*, vol. 26, no. 4, pp. 1119–1126, 1998.

[11] R. Petr *et al.*, "Performance summary on a high power dense plasma focus x-ray lithography point source producing 70 nm line features in AlGaAs microcircuits," *Review of scientific instruments*, vol. 75, no. 8, pp. 2551–2559, 2004.

[12] D. Wong, A. Patran, T. Tan, R. Rawat, and P. Lee, "Soft X-ray optimization studies on a dense plasma focus device operated in neon and argon in repetitive mode," *IEEE Transactions on plasma science*, vol. 32, no. 6, pp. 2227–2235, 2004.

[13] F. Castillo-Mejía, M. M. Milanese, R. L. Moroso, J. O. Pouzo, and M. A. Santiago, "Small plasma focus studied as a source of hard X-ray," *IEEE transactions on plasma science*, vol. 29, no. 6, pp. 921–926, 2001.
[14] R. Rawat *et al.*, "Soft X-ray imaging using a neon filled plasma focus X-ray source," *Journal of fusion energy*, vol. 23, pp. 49–53, 2004.
[15] F. Beg, I. Ross, A. Lorenz, J. Worley, A. Dangor, and M. Haines, "Study of x-ray emission from a table top plasma focus and its application as an x-ray backlighter," *Journal of Applied Physics*, vol. 88, no. 6, pp. 3225–3230, 2000.
[16] S. Hussain, M. Shafiq, R. Ahmad, A. Waheed, and M. Zakaullah, "Plasma focus as a possible x-ray source for radiography," *Plasma Sources Science and Technology*, vol. 14, no. 1, p. 61, 2005.
[17] V. A. Gribkov, A. Srivastava, P. L. C. Keat, V. Kudryashov, and S. Lee, "Operation of NX2 dense plasma focus device with argon filling as a possible radiation source for micro-machining," *IEEE transactions on plasma science*, vol. 30, no. 3, pp. 1331–1338, 2002.
[18] M. Akel, S. Lee, and S. H. Saw, "Numerical Experiments in Plasma Focus Operated in Various Gases," *IEEE Trans. Plasma Sci.*, vol. 40, no. 12, pp. 3290–3297, Dec. 2012, doi: 10.1109/TPS.2012.2220863.
[19] S. Lee, "Plasma Focus Radiative Model: Review of the Lee Model Code," *J Fusion Energ*, vol. 33, no. 4, pp. 319–335, Aug. 2014, doi: 10.1007/s10894-014-9683-8.
[20] "The Universal Plasma Focus Machine." Accessed: Nov. 21, 2025. [Online]. Available: https://www.plasmafocus.net/IPFS/modelpackage/UPF.htm
[21] S. Lee, *Radiations in Plasmas*. 978, 1984.
[22] S. H. Saw, "Experimental Studies of a Current-stepped Z-pinch," 1990.
[23] S. Lee, "A sequential plasma focus," *IEEE transactions on plasma science*, vol. 19, no. 5, pp. 912–919, 1991.
[24] S. Lee and A. Serban, "Dimensions and lifetime of the plasma focus pinch," *IEEE Transactions on plasma science*, vol. 24, no. 3, pp. 1101–1105, 1996.
[25] S. Lee *et al.*, "A simple facility for the teaching of plasma dynamics and plasma nuclear fusion," *American Journal of Physics*, vol. 56, no. 1, pp. 62–68, 1988.
[26] T. Tou, S. Lee, and K. Kwek, "Nonperturbing plasma-focus measurements in the run-down phase," *IEEE Transactions on Plasma Science*, vol. 17, no. 2, pp. 311–315, 1989.
[27] J. Ali, "Development and studies of a small plasma focus," *Ph. D. Dissertation*, 1990.
[28] Sor Heoh Saw, P. C. K. Lee, R. S. Rawat, and Sing Lee, "Optimizing UNU/ICTP PFF Plasma Focus for Neon Soft X-ray Operation," *IEEE Trans. Plasma Sci.*, vol. 37, no. 7, pp. 1276–1282, July 2009, doi: 10.1109/TPS.2009.2022167.
[29] C. Pavez and L. Soto, "Demonstration of X-ray emission from an ultraminiature pinch plasma focus discharge operating at 0.1 J nanofocus," *IEEE Transactions on Plasma Science*, vol. 38, no. 5, pp. 1132–1135, 2010.
[30] "The Universal Plasma Focus Machine." Accessed: Feb. 08, 2024. [Online]. Available: https://www.plasmafocus.net/IPFS/modelpackage/UPF.htm
[31] N. V. Zavyalov *et al.*, "A source with a 1013 DT neutron yield on the basis of a spherical plasma focus chamber," *Plasma Phys. Rep.*, vol. 39, no. 3, pp. 243–247, Mar. 2013, doi: 10.1134/S1063780X12120070.
[32] V. V. Maslov *et al.*, "A KPU-200 movable capacitor installation," *Instrum Exp Tech*, vol. 57, no. 2, pp. 131–134, Mar. 2014, doi: 10.1134/S0020441214010254.
[33] "The Plasma Focus—Numerical Experiments, Insights and Applications | SpringerLink." Accessed: Nov. 21, 2025. [Online]. Available: https://link.springer.com/chapter/10.1007/978-981-10-4217-1_3